

Application of Lattice Boltzmann Method to Simulation of Compressible Turbulent Flow

Congshan Zhuo¹, Chengwen Zhong^{1,2}, Kai Li¹, Shengwei Xiong¹, Xiaopeng Chen³ and Jun Cao^{4,*}

¹ National Key Laboratory of Science and Technology on Aerodynamic Design and Research, Northwestern Polytechnical University, Xi'an, Shaanxi 710072, China.

² Center for High Performance Computing, Northwestern Polytechnical University, Xi'an, Shaanxi 710072, China.

³ School of Mechanics, Civil Engineering and Architecture, Northwestern Polytechnical University, Xi'an, Shaanxi 710072, China.

⁴ Department of Mechanical and Industrial Engineering, Ryerson University, Toronto, Ontario, M5B 2K3, Canada.

Received 30 January 2010; Accepted (in revised version) 7 May 2010

Communicated by Rho Shin Myong

Available online 23 June 2010

Abstract. The main goal of this paper is to develop the coupled double-distribution-function (DDF) lattice Boltzmann method (LBM) for simulation of subsonic and transonic turbulent flows. In the present study, we adopt the second-order implicit-explicit (IMEX) Runge-Kutta schemes for time discretization and the Non-Oscillatory and Non-Free-Parameters Dissipative (NND) finite difference scheme for space discretization. The Sutherland's law is used for expressing the viscosity of the fluid due to considerable temperature change. Also, the Spalart-Allmaras (SA) turbulence model is incorporated in order for the turbulent flow effect to be pronounced. Numerical experiments are performed on different turbulent compressible flows around a NACA0012 airfoil with body-fitted grid. Our numerical results are found to be in good agreement with experiment data and/or other numerical solutions, demonstrating the applicability of the method presented in this study to simulations of both subsonic and transonic turbulent flows.

AMS subject classifications: 76M28, 82B40, 76N15, 76F55

Key words: Lattice Boltzmann method, compressible turbulent flow, airfoil, body-fitted grid.

*Corresponding author. *Email addresses:* zhuocs@mail.nwpu.edu.cn (C. Zhuo), zhongcw@nwpu.edu.cn (C. Zhong), li040384@mail.nwpu.edu.cn (K. Li), xiongshengwei@mail.nwpu.edu.cn (S. Xiong), xchen76@nwpu.edu.cn (X. Chen), jcao@ryerson.ca (J. Cao)

1 Introduction

The Lattice Boltzmann method (LBM) has recently attracted an increasing amount of attention from the computational fluid dynamics (CFD) community [1, 2]. The LBM is a derivative of the lattice gas automata (LGA) method with some advantages of the LGA successfully inherited. Different from the conventional numerical methods for solving the macroscopic governing equations, the LBM is based on microscopic models and the kinetic theories [3]. The mechanism of LBM is parallel in nature due to the locality of particle interaction and the transport of particle information, so it is well suitable for massively parallel computing. Moreover, the LBM has some other advantages, such as good numerical robustness, flexibility with respect to complex boundaries, and computational efficiency.

As of today, the LBM has achieved great success in simulating semi-incompressible and isothermal fluid flows. Available literatures also reveal that the LBM has been successfully applied to the solution of the Euler [4–7] or Navier-Stokes (N-S) equations [8–22] for a compressible fluid. For instance, Qu et al. [7] proposed a non-free-parameter LBM to construct equilibrium distribution functions for inviscid compressible flows at high Mach number. Sun et al. [10–13] developed a locally adaptive lattice Boltzmann model suitable for flows in a wide range of Mach numbers for compressible flows. Watari [15] proposed finite difference lattice Boltzmann method (FDLBM) for numerical simulations of flows from subsonic to supersonic ranges for both inviscid (Euler model) and viscous (Navier-Stokes model) fluids. Yan et al. [4, 17] presented a compressible LBM with three-speed and three-energy-level for the Euler [4] and Navier-Stokes equations [17]. Pan et al. [18] and Gan et al. [19] also worked on improving lattice Boltzmann model for some high-speed inviscid and viscous supersonic flow cases, respectively, with higher Mach numbers (up to 30 or a bit above). Recently, Li Q [20], Wang Y et al. [21] developed a coupled double-distribution-function (DDF) LBM by combining the DDF approach and the multi-speed approach, and used it to simulate compressible fluid flow with arbitrary specific-heat ratio and Prandtl number. In this method, a density distribution function based on a multi-speed lattice as well as a total energy distribution function are used, and these two distribution functions are coupled together via the state equation. In [20], Li Q et al. applied two different methods to construct equilibrium distribution functions in two coupled DDF models, respectively. Model 1 is based on the truncated Maxwellian distribution function and limited to low- and moderate-Mach-number viscous fluid flows; Model 2 is based on a circular function [7] and can be used to simulate viscous fluid flows with high Mach numbers. In the two models, the density distribution function is used to recover the compressible continuity and momentum equations, while the energy equation is recovered by a total energy distribution function. The total energy distribution function is coupled with the density distribution function via the ideal gas law. This method can be used for non-uniform grid through the transformation of coordinates [22].

Most flows encountered in engineering applications are of turbulent nature. The pre-

diction of flow phenomena such as boundary layer separation depends strongly on the choice of the turbulence model. In combination with other models used for turbulent flow studies, the LBM approach has been considered for simulation of realistic compressible fluid flows with turbulence effects taken into account. For example, by incorporating two-layer mixing-length algebraic model and two versions (standard and renormalization group (RNG)) of the κ - ϵ two-equation model into the lattice Boltzmann method, Teixeira [23] successfully simulated turbulent flow in a straight pipe. In extension of this strategy, Filippova et al. [24] proposed multi-scale lattice Boltzmann schemes and performed numerical investigation of turbulent flow associated with complex curvilinear geometry; Imamura et al. [25] presented the generalized form of interpolation supplemented lattice Boltzmann method and applied it to simulations of turbulent flows around a NACA0012 airfoil. On the other hand, in connection with the very large eddy simulation (VLES) approach, the LBM was developed for turbulent flow simulation; some typical research work in this direction can be found in [26–30].

Apart from the above-mentioned choices, one-equation models such as the Spalart-Allmaras (SA) turbulence model [31–33] seem to be an ideal compromise between algebraic and two-equation models. It does not require finer grid resolution near the wall; thus, the computation cost using the one-equation SA model is lessened when compared to using the two-equation model. In particular, the SA model became quite popular because of its satisfactory results for a wide range of flow problems and its reliable numerical properties. Using conventional numerical methods, such as finite difference and finite volume approaches, this model has provided good simulation results for transonic turbulent flow around a full aircraft configuration [32] and for supersonic flow associated with other complex configurations [33]. In order to solve the turbulent compressible flow problems, the SA model is incorporated into the coupled DDF models in this paper. The simulation using a body-fitted grid is then performed for turbulent compressible flows around NACA0012 airfoil at subsonic and transonic regimes, respectively.

The rest of the paper is organized as follows. The LBM model and different versions of the SA turbulence model are described in detail in the Section 2. In Section 3, selected numerical simulation results are shown to demonstrate the reliability and effectiveness of the present model. Finally, concluding remarks are made in Section 4.

2 Numerical methods

2.1 LBM for compressible fluid flow

The discrete Boltzmann Bhatnagar-Gross-Krook (BGK) equation reads [34]

$$\frac{\partial f_\alpha}{\partial t} + (\vec{e}_\alpha \cdot \vec{\nabla}) f_\alpha = -\frac{1}{\tau_f} (f_\alpha - f_\alpha^{eq}), \quad (2.1)$$

where f_α is the density distribution function, f_α^{eq} is the corresponding equilibrium distribution function, \vec{e}_α is the discrete particle velocity along the α -th direction, and τ_f is the

relaxation time for the momentum transport. In this study, two-dimensional problems are considered, leading Eq. (2.1) to

$$\frac{\partial f_\alpha}{\partial t} + \left(e_{\alpha x} \frac{\partial f_\alpha}{\partial x} + e_{\alpha y} \frac{\partial f_\alpha}{\partial y} \right) = -\frac{1}{\tau_f} (f_\alpha - f_\alpha^{eq}), \tag{2.2}$$

with $\vec{e}_\alpha = (e_{\alpha x}, e_{\alpha y})^t$. In order to deal with the non-uniform grid, a computational plane ($\vec{\xi} = (\xi, \eta)^t$) is employed. For simplification, the grid spacing of the uniform rectangular grid on the computational plane, $\Delta\xi$ and $\Delta\eta$, are set as 1; Δx and Δy , corresponding to the physical plane ($\vec{x} = (x, y)^t$), are normally non-uniform. The relationship between $\vec{\xi}$ and \vec{x} satisfies the following condition [35]:

$$\begin{bmatrix} \frac{\partial \xi}{\partial x} & \frac{\partial \xi}{\partial y} \\ \frac{\partial \eta}{\partial x} & \frac{\partial \eta}{\partial y} \end{bmatrix} = \frac{1}{J} \begin{bmatrix} \frac{\partial y}{\partial \eta} & -\frac{\partial x}{\partial \eta} \\ -\frac{\partial y}{\partial \xi} & \frac{\partial x}{\partial \xi} \end{bmatrix}, \tag{2.3}$$

where the Jacobian determinant J is denoted by

$$J = \frac{\partial x}{\partial \xi} \frac{\partial y}{\partial \eta} - \frac{\partial x}{\partial \eta} \frac{\partial y}{\partial \xi}. \tag{2.4}$$

Using the chain rule of differentiation, the convection term in the Eq. (2.2) can be rewritten as

$$\begin{aligned} e_{\alpha x} \frac{\partial f_\alpha}{\partial x} + e_{\alpha y} \frac{\partial f_\alpha}{\partial y} &= e_{\alpha x} \left(\frac{\partial f_\alpha}{\partial \xi} \frac{\partial \xi}{\partial x} + \frac{\partial f_\alpha}{\partial \eta} \frac{\partial \eta}{\partial x} \right) + e_{\alpha y} \left(\frac{\partial f_\alpha}{\partial \xi} \frac{\partial \xi}{\partial y} + \frac{\partial f_\alpha}{\partial \eta} \frac{\partial \eta}{\partial y} \right) \\ &= \left(e_{\alpha x} \frac{\partial \xi}{\partial x} + e_{\alpha y} \frac{\partial \xi}{\partial y} \right) \frac{\partial f_\alpha}{\partial \xi} + \left(e_{\alpha x} \frac{\partial \eta}{\partial x} + e_{\alpha y} \frac{\partial \eta}{\partial y} \right) \frac{\partial f_\alpha}{\partial \eta} \\ &= \tilde{e}_{\alpha \xi} \frac{\partial f_\alpha}{\partial \xi} + \tilde{e}_{\alpha \eta} \frac{\partial f_\alpha}{\partial \eta}, \end{aligned} \tag{2.5}$$

where $\tilde{e}_{\alpha \xi}$, $\tilde{e}_{\alpha \eta}$ are the contravariant velocity [25] in the computational plane and defined as

$$\tilde{e}_{\alpha \xi} = e_{\alpha x} \frac{\partial \xi}{\partial x} + e_{\alpha y} \frac{\partial \xi}{\partial y}, \tag{2.6a}$$

$$\tilde{e}_{\alpha \eta} = e_{\alpha x} \frac{\partial \eta}{\partial x} + e_{\alpha y} \frac{\partial \eta}{\partial y}, \tag{2.6b}$$

then, Eq. (2.2) can be rewritten as

$$\frac{\partial f_\alpha}{\partial t} + \left(\tilde{e}_{\alpha \xi} \frac{\partial f_\alpha}{\partial \xi} + \tilde{e}_{\alpha \eta} \frac{\partial f_\alpha}{\partial \eta} \right) = -\frac{1}{\tau_f} (f_\alpha - f_\alpha^{eq}), \tag{2.7}$$

Eq. (2.7) is the evolution equation for the density distribution function on the body-fitted coordinate systems. The evolution equation of the total energy distribution function is expressed as follows [20,36]:

$$\frac{\partial h_\alpha}{\partial t} + (\vec{e}_\alpha \cdot \vec{\nabla}) h_\alpha = -\frac{1}{\tau_h} (h_\alpha - h_\alpha^{eq}) + \frac{1}{\tau_{hf}} \left(\vec{e}_\alpha \cdot \vec{u} - \frac{|\vec{u}|^2}{2} \right) (f_\alpha - f_\alpha^{eq}), \quad (2.8)$$

where h_α is the total energy distribution function; h_α^{eq} is the corresponding equilibrium distribution function; and

$$\tau_{hf} = \frac{\tau_h \tau_f}{\tau_f - \tau_h},$$

with τ_h denoting the total energy relaxation time. After utilizing Eqs. (2.5) and (2.6), Eq. (2.8) can be transformed to

$$\frac{\partial h_\alpha}{\partial t} + \left(\tilde{e}_{\alpha\xi} \frac{\partial h_\alpha}{\partial \xi} + \tilde{e}_{\alpha\eta} \frac{\partial h_\alpha}{\partial \eta} \right) = -\frac{1}{\tau_h} (h_\alpha - h_\alpha^{eq}) + \frac{1}{\tau_{hf}} \left(\vec{e}_\alpha \cdot \vec{u} - \frac{|\vec{u}|^2}{2} \right) (f_\alpha - f_\alpha^{eq}). \quad (2.9)$$

Note that we can solve Eq. (2.7) and Eq. (2.9) on the body-fitted coordinate systems which are the same as on the uniform grid. In the present paper, we adopt the second-order IMEX Runge-Kutta scheme [20, 37] for time discretization, which consist of an implicit step for the collision term and an explicit one for the other terms. In order to capture discontinuities, the Non-Oscillatory and Non-Free-Parameters Dissipative (NND) finite difference scheme [7, 22, 38] is adopted to evaluate the convection terms. The details of such methods can be found in [7,20,22,37,38]. The macroscopic quantities such as density ρ , velocity \vec{u} and temperature T can be calculated using

$$\rho = \sum_\alpha f_\alpha, \quad \vec{u} = \frac{1}{\rho} \sum_\alpha f_\alpha \vec{e}_\alpha, \quad T = \frac{2}{bR} \left(\frac{1}{\rho} \sum_\alpha h_\alpha - \frac{|\vec{u}|^2}{2} \right), \quad (2.10)$$

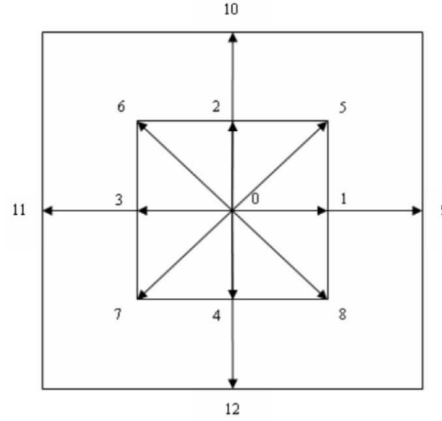
where b is a constant which is related to the specific-heat ratio γ by $\gamma = (b+2)/b$. Then, the relaxation times τ_f and τ_h are computed as follows:

$$\tau_f = \frac{\mu}{p}, \quad \tau_h = \frac{\tau_f}{Pr} = \frac{1}{p} \frac{\mu}{Pr}, \quad (2.11)$$

where Pr is the Prandtl number and μ is the dynamic viscosity. For the compressible fluid flows with great variation of temperature, the impact of temperature upon the viscosity should be considered through application of the Sutherland's law

$$\mu = \mu_\infty \left(\frac{T}{T_\infty} \right)^{\frac{3}{2}} \frac{T_\infty + S}{T + S}, \quad (2.12)$$

where $T_\infty = 288.15K$ and $S = 110.4K$.

Figure 1: Discrete velocities of the $D2Q13$ lattice.

Because the original $D2Q9$ model cannot recover the compressible fluid momentum equation, a 2-dimensional and 12-velocity ($D2Q12$, model 1) or $D2Q13$ (model 2) square lattice, as shown in Fig. 1, is used with \vec{e}_α defined as

$$\vec{e}_\alpha = \begin{cases} \{0,0\}^t, & \alpha=0, \text{ only for } D2Q13, \\ c\{\cos[(\alpha-1)\pi/2], \sin[(\alpha-1)\pi/2]\}^t, & \alpha=1,2,3,4, \\ \sqrt{2}c\{\cos[(2\alpha-1)\pi/4], \sin[(2\alpha-1)\pi/4]\}^t, & \alpha=5,6,7,8, \\ 2c\{\cos[(\alpha-9)\pi/2], \sin[(\alpha-9)\pi/2]\}^t, & \alpha=9,10,11,12, \end{cases} \quad (2.13)$$

where $c = \sqrt{RT_c}$ is the characteristic speed of the lattice fluid with T_c denoting the characteristic temperature.

As aforementioned, the equilibrium distribution functions in the model 1 are based on the truncated Maxwellian distribution functions, those in the model 2 are based on the circular functions which are distributed to the lattice velocity directions by Lagrangian interpolation. Relevant details can be found in [7, 20]. The equilibrium total energy distribution function is expressed as [20]:

$$h_\alpha^{eq} = [E + (\vec{e}_\alpha - \vec{u}) \cdot \vec{u}] f_\alpha^{eq} + \omega_\alpha \frac{p}{c^2} RT, \quad (2.14)$$

where $E = (bRT + |\vec{u}|^2)/2$ is the total energy, $\omega_0 = 0$, $\omega_{1,2,3,4} = -1/3$, $\omega_{5,6,7,8} = 1/4$ and $\omega_{9,10,11,12} = 1/12$. The density and total energy distribution functions are coupled by using the ideal gas law $p = \rho RT$.

2.2 Turbulence model

In order to solve the turbulent compressible flow problems, the Spalart-Allmaras turbulence model is employed. The SA model is a one-equation model which solves a transport equation for a transformed eddy kinematic viscosity $\tilde{\nu}$ related to ν_t . The original SA

model is expressed as [31, 33, 38]:

$$\frac{D\tilde{v}}{Dt} = C_{b_1}(1-f_{t_2})\tilde{S}\tilde{v} + \frac{1}{\sigma} \left[\vec{\nabla} \cdot ((\nu_l + \tilde{v})\vec{\nabla}\tilde{v}) + C_{b_2}|\vec{\nabla}\tilde{v}|^2 \right] - \left(C_{w_1}f_w - \frac{C_{b_1}}{\kappa^2}f_{t_2} \right) \left(\frac{\tilde{v}}{d} \right)^2, \quad (2.15)$$

where ν_l is the laminar kinematic viscosity. The eddy kinematic viscosity ν_t is defined as:

$$\nu_t = \tilde{v}f_{\nu_1}, \quad f_{\nu_1} = \frac{\chi^3}{\chi^3 + C_{\nu_1}^3}, \quad \chi = \frac{\tilde{v}}{\nu_l},$$

then, the turbulent dynamic viscosity is computed using $\mu_t = \rho\nu_t$. The calculation involves the following parameters

$$\begin{aligned} f_{t_2} &= C_{t_3} \exp(-C_{t_4}\chi^2), & \tilde{S} &= \sqrt{2\Omega_{ij}\Omega_{ij}f_{v_3} + \frac{\tilde{v}}{\kappa^2 d^2}f_{v_2}}, \\ \Omega_{ij} &= \frac{1}{2} \left(\frac{\partial u_i}{\partial x_j} - \frac{\partial u_j}{\partial x_i} \right), & f_{v_2} &= 1 - \frac{\chi}{1 + \chi f_{v_1}}, & f_{v_3} &= 1, \\ f_w &= g \left(\frac{1 + C_{w_3}^6}{g^6 + C_{w_3}^6} \right)^{\frac{1}{6}}, & g &= r + C_{w_2}(r^6 - r), & r &= \frac{\tilde{v}}{\tilde{S}\kappa^2 d^2}. \end{aligned}$$

Constants used in the model are

$$\begin{aligned} C_{b_1} &= 0.1355, & C_{b_2} &= 0.622, & \sigma &= 2/3, & \kappa &= 0.41, & C_{w_1} &= \frac{C_{b_1}}{\kappa^2} + \frac{1 + C_{b_2}}{\sigma}, \\ C_{w_2} &= 0.3, & C_{w_3} &= 2, & C_{\nu_1} &= 7.1, & C_{t_3} &= 1.1, & C_{t_4} &= 2. \end{aligned}$$

To improve the convergence of the residual turbulence, Spalart proposed the following modifications [33]:

$$\tilde{S} = \sqrt{2\Omega_{ij}\Omega_{ij}f_{v_3} + \frac{\tilde{v}}{\kappa^2 d^2}f_{v_2}},$$

with

$$f_{v_2} = \left(1 + \frac{\chi}{C_{v_2}} \right)^{-3}, \quad f_{v_3} = \frac{(1 + \chi f_{v_1})(1 - f_{v_2})}{\chi}, \quad C_{v_2} = 5, \quad \chi = \max\{\chi, 10^{-4}\}.$$

In order to adapt the model to compressible fluid flows, the convection term in Eq. (2.15) is modified

$$\frac{\partial \tilde{v}}{\partial t} + \frac{\partial}{\partial x_j}(\tilde{v}u_j) = \frac{D\tilde{v}}{Dt} + \tilde{v}\vec{\nabla} \cdot \vec{u} = RHS, \quad (2.16)$$

where the right hand side (RHS) is the same as in Eq. (2.15).

Finally, the modified SA model is re-written as follows:

$$\begin{aligned} \frac{D\tilde{v}}{Dt} &= \left[C_{b_1}(1-f_{t_2})\tilde{S} - \vec{\nabla} \cdot \vec{u} \right] \tilde{v} + \frac{1}{\sigma} \left[\vec{\nabla} \cdot ((\nu_l + \tilde{v})\vec{\nabla}\tilde{v}) + C_{b_2}|\vec{\nabla}\tilde{v}|^2 \right] \\ &\quad - \left(C_{w_1}f_w - \frac{C_{b_1}}{\kappa^2}f_{t_2} \right) \left(\frac{\tilde{v}}{d} \right)^2. \end{aligned} \quad (2.17)$$

In this study, the modified SA model is used and, accordingly, variables are modified as

$$\mu = \mu_l + \mu_t, \quad \frac{\mu}{Pr} = \frac{\mu_l}{Pr_l} + \frac{\mu_t}{Pr_t}, \quad (2.18)$$

where the subscripts l and t represent laminar and turbulent contributions, respectively. In all simulations of the air flows included in this paper, Pr_l and Pr_t are equal to 0.72 and 0.9, respectively. Combining Eq. (2.11) with Eq. (2.18), the relaxation times τ_f and τ_h should be re-computed using

$$\tau_f = \frac{\mu_l + \mu_t}{p}, \quad \tau_h = \frac{1}{p} \left(\frac{\mu_l}{Pr_l} + \frac{\mu_t}{Pr_t} \right), \quad (2.19)$$

where μ_l is computed using Eq. (2.12).

3 Numerical results

The numerical simulations are performed for the turbulent compressible flow around a NACA0012 airfoil. In this study, a body-fitted (C-type) grid with resolution of 257×65 is used. With the chord length as unit length, the computational domain is shown in Fig. 2. Details of the grid in the vicinity of the airfoil are shown in Fig. 3, with 173 points on the surface of airfoil. The thickness of the first layer adjacent to the wall of the airfoil is 1.4×10^{-4} for code validation (see Section 3.1), and then is 2.4×10^{-5} for other numerical experiments with fluid viscosity particularly taken into account by employing the SA model (see Section 3.2). Since the numerical experiments conducted in the present study aim mainly at verifying the applicability and robustness of the code we developed, the mesh is generated with no particular treatment to intentionally accommodate shocks possibly incurred by the incoming subsonic or transonic flows, except that the wake area is distributed with reasonably dense nodes.

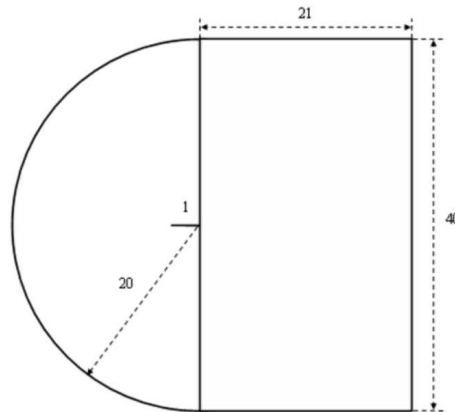


Figure 2: Computational domain.

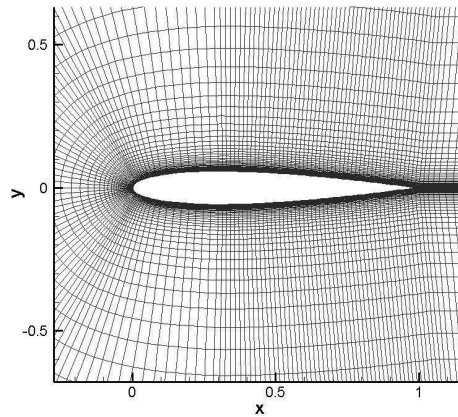


Figure 3: C-type grid of NACA0012 airfoil (257×65).

The reference density ρ_0 and the reference temperature $T_0 = 288.15K$ are used in simulations and the reference velocity and the reference pressure are defined as

$$u_0 = \sqrt{\gamma RT_0}, \quad P_0 = \rho_0 RT_0,$$

while $\mu = 1.789 \times 10^{-5} \text{kg}/(\text{m}\cdot\text{s})$. In this study, these reference values are taken corresponding to the incoming free stream.

3.1 Code validation

The first test is performed for a slightly inclined subsonic flow ($Ma=0.85$, $\alpha=1.0^\circ$) around a NACA0012 airfoil. In this simulation, the SA model is not included and the reflective-wall boundary condition applies to the wall; that is, two layers of ghost nodes inside the wall are used and the mirror method is employed to obtain the distribution functions [7]. Moreover, the non-equilibrium-extrapolation method [39] for the distribution functions is applied on the airfoil surface. Free stream condition is applied at the outer boundary (the distribution functions are always set as in their equilibrium states). Fig. 4 shows the surface pressure coefficients compared with the results of AGARD extracted from [40] and [41]. The numerical results of the two present models are found to be generally in good agreement with the results from different resources. It is noticed that the two present models can predict the shock locations, though the shock location on the lower surface of the airfoil is not sufficiently precisely captured if compared with the weighted essentially nonoscillatory (WENO) approach as shown in Fig. 4. The main reason could be that the accuracy of discretization scheme adopted in the present models is in a lower order than that taken by others. In [41], the third-order IMEX Runge-Kutta scheme and the fifth-order WENO scheme are used for time discretization and space discretization, respectively, but the computation time also increases by 50% compared with the two models employed here.

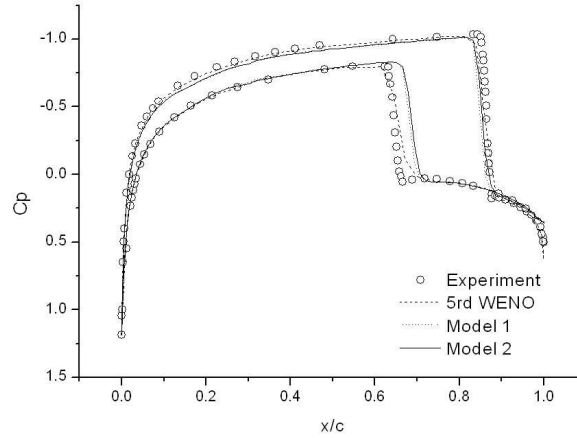


Figure 4: C_p distribution along surface of airfoil NACA0012 at $Ma=0.85$, $\alpha=1.0^\circ$.

3.2 Turbulent compressible flow

The subsonic and transonic turbulent flows around a NACA0012 airfoil are simulated in order to demonstrate the applicability of the present method coupling the LBM model with the SA turbulence model. From extensive available experimental data, two cases are selected with $Ma = 0.503$, 0.775 , $Re = 2.85 \times 10^6$, 1.0×10^7 and angles of attack $\alpha = 8.02^\circ$, 2.05° , respectively, for the two simulations. In these tests, the wall boundary condition for viscous fluid flow (adiabatic and no-slip boundary condition) is applied at the airfoil surface. Two layers of ghost nodes inside the wall are used, and the anti-symmetry method is used for the distribution functions as follows:

$$f_{\alpha,i,-1} = f_{anti(\alpha),i,1}, \quad f_{\alpha,i,-2} = f_{anti(\alpha),i,2}, \quad (3.1)$$

where nodes -1 and -2 are the ghost nodes of nodes 1 and 2 , respectively and $anti(\alpha)$ signifies the opposite direction of α . Other boundary conditions are the same as those used for code validation.

Fig. 5 shows the surface pressure coefficient comparisons with the experimental data [42, 43] at $Ma = 0.503$ and $Ma = 0.775$, respectively. Fig. 5(a) demonstrates models 1 and 2 are both working, without noticeable discrepancy, for simulation of subsonic turbulent flow. From Fig. 5(b) corresponding to the transonic flow simulation, we can find that the result obtained from model 2 is slightly better than the result obtained from model 1 when both are compared against the experimental data. It is however noticed that, for both subsonic and transonic flow simulations, the pressure coefficient near the trailing edge does not look sufficiently smooth. This is because both simulations share an identical mesh and the mesh is not particularly refined in the vicinity of the trailing edge that is followed by the wake region. Through a further numerical investigation using a mesh with enriched density of nodes over the wake area, it has been confirmed that the pressure coefficient gets smoothed near the trailing edge. As aforementioned, the goal of

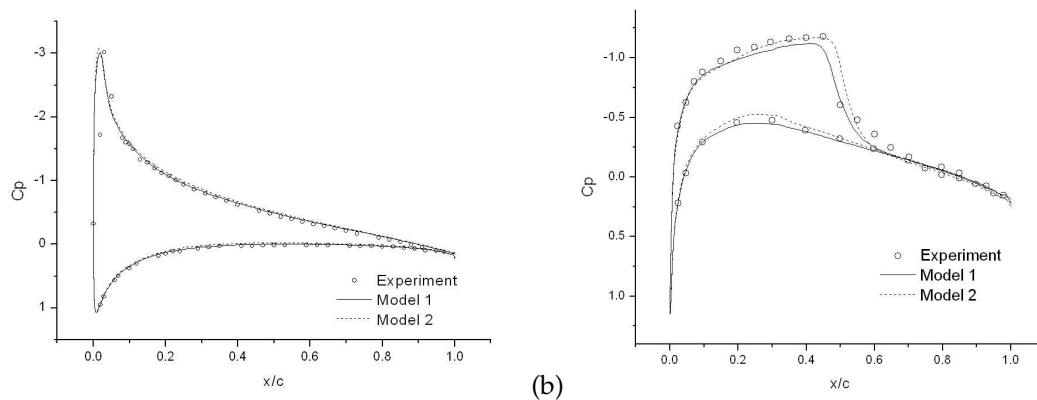


Figure 5: C_p distribution along surface of airfoil NACA0012 at (a) $Ma=0.503$, $Re=2.85 \times 10^6$, $\alpha=8.02^\circ$; and (b) $Ma=0.775$, $Re=1.0 \times 10^7$, $\alpha=2.05^\circ$.

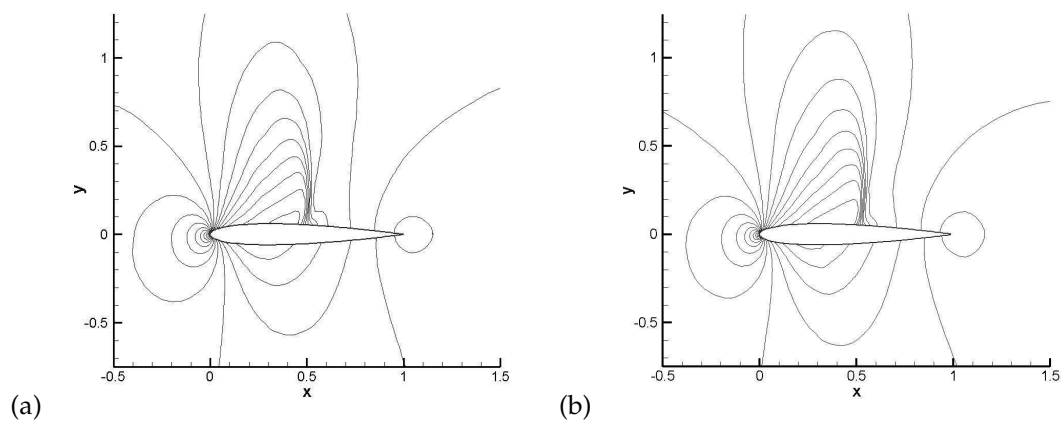


Figure 6: Pressure contours at $Ma=0.775$, $Re=1.0 \times 10^7$, $\alpha=2.05^\circ$. (a): Model 1; (b): Model 2.

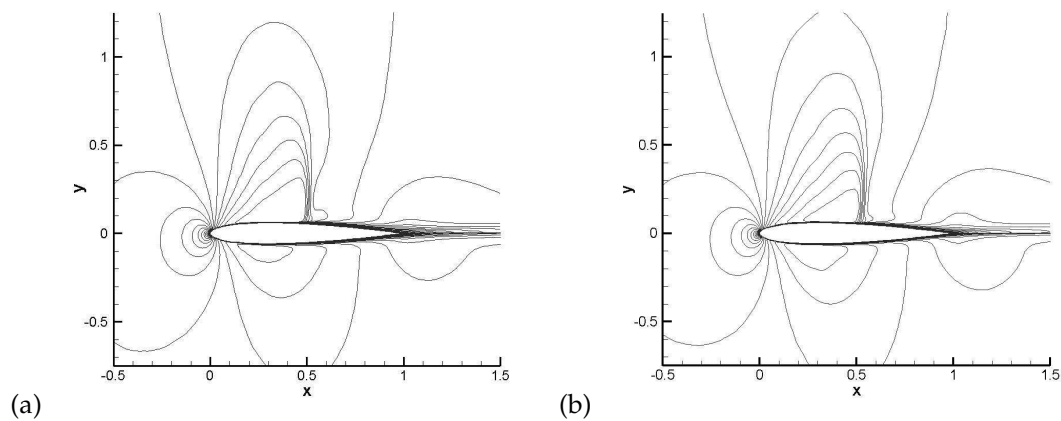


Figure 7: Contours of velocity magnitude at $Ma=0.775$, $Re=1.0 \times 10^7$, $\alpha=2.05^\circ$. (a): Model 1; (b): Model 2.

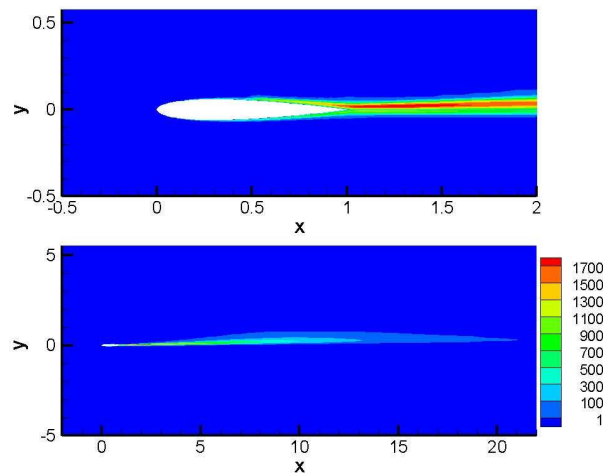


Figure 8: Viscosity ratio contours at $Ma=0.775$, $Re=1.0 \times 10^7$, $\alpha=2.05^\circ$ (Model 1).

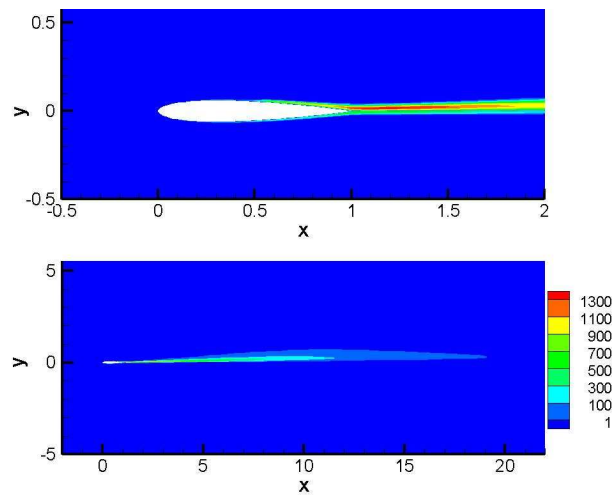


Figure 9: Viscosity ratio contours at $Ma=0.775$, $Re=1.0 \times 10^7$, $\alpha=2.05^\circ$ (Model 2).

this study is to test the robustness of the method coupling the DDF with the SA model for simulation of turbulent compressible flows without requesting a case-dependent mesh. Here, Fig. 5 reveals that our method can satisfactorily deal with both subsonic and transonic flow cases on an identical ordinary mesh. Besides, Fig. 5 also demonstrates that the results obtained by the present models are in excellent agreement with the experimental data [42, 43].

In order to look into the performance of the two models presented in this study, Figs. 6-10 are used to compare the pressure, magnitude of velocity, and viscosity ratio contours at $Ma=0.775$ using the two different models. Each two consecutive iso-value lines for dimensionless pressure or velocity magnitude are in difference of 0.05 for each

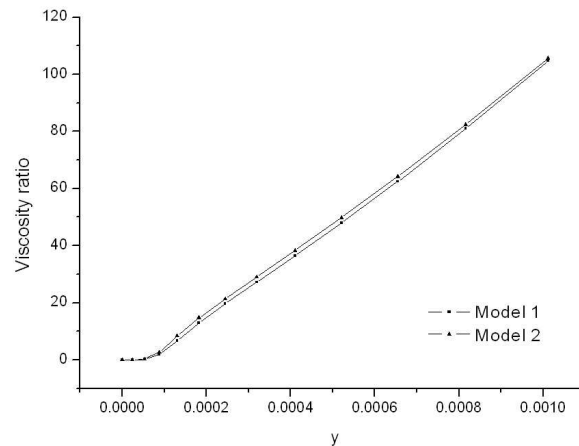


Figure 10: Distribution of viscosity ratio at the trailing edge along the line normal to the upper surface of airfoil at $Ma=0.775$, $Re=1.0 \times 10^7$, $\alpha=2.05^\circ$.

of Figs. 6-7. The comparisons of the pressure (Fig. 6) and the velocity magnitude (Fig. 7) indicate that the two models can produce practically identical results for transonic flow simulation, except that some slight discrepancies can be found near the shock on the upper surface and at the position near one quarter of the chord length on the lower surface. Such discrepancies echo the slight differences in pressure coefficients resulting from the two models, as already demonstrated in Fig. 5(b).

Finally, Figs. 8 and 9 show the viscosity ratio contours at $Ma=0.775$ corresponding to the two models, respectively. It is noticed that the viscosity ratio reaches its maximum within the wake region on both figures. Also, no significant difference can be found in the behaviors of the turbulence obtained by using two different models. Even when zooming in the sensitive trailing edge area, Fig. 10 depicts the distribution of viscosity ratios for the two models along the line on the grid that is starting at the trailing edge and normal to the upper surface of airfoil; again, as anticipated, the viscosity ratio distributions in this sensitive area are almost identical for the two different models.

4 Conclusions

In this paper, we incorporate the Spalart-Allmaras (SA) turbulent model into the coupled double-distribution-function (DDF) lattice Boltzmann method (LBM), while the Sutherland's law is used for updating the viscosity due to temperature changes. This enhanced LBM is then applied to the simulation of subsonic and transonic turbulent flows around a NACA0012 airfoil. Two models are evaluated, and the numerical results demonstrate that both models can provide good prediction of shock location and accurate resolution of the compressible turbulent flows without significant difference. All numerical results appear in fairly good agreements with experimentally obtained data, indicating that our

method can be used for simulating both subsonic and transonic turbulent flows. Moreover, the two sets of test cases corresponding to subsonic and transonic turbulent flows employ an identical mesh without any adaptation. Thus, the method exhibits a remarkable generality in practical applications, and it looks promising for simulations of subsonic and transonic turbulent flows of more practical interests.

Acknowledgments

This project was financially supported mainly by the Aeronautical Science Fund of China (Grant No. 20061453020). The funds from the Foundation for Basic Research of Northwestern Polytechnical University, P. R. China, as well as from the Discovery Grant of the Natural Sciences and Engineering Research Council of Canada (NSERC) were also used to support this research work.

References

- [1] S. Chen and G. D. Doolen, Lattice Boltzmann method for fluid flows, *Annu. Rev. Fluid. Mech.*, 30 (1998), 329–364.
- [2] S. Succi, *Lattice Boltzmann Equation for Fluid Dynamics and Beyond*, Clarendon Press, Oxford, 2001.
- [3] S. Hou, Q. Zou, S. Chen, G. D. Doolen and A. C. Cogley, Simulation of cavity flow by the lattice Boltzmann method, *J. Comput. Phys.*, 118 (1995), 329–347.
- [4] G. Yan, Y. Chen and S. Hu, Simple lattice Boltzmann model for simulating flows with shock wave, *Phys. Rev. E.*, 59 (1999), 454–459.
- [5] W. Shi, W. Shyy and R. W. Mei, Finite-difference-based lattice Boltzmann method for inviscid compressible flows, *Numer. Heat. Tr. B-Fund.*, 40 (2001), 1–21.
- [6] T. Kataoka and M. Tsutahara, Lattice Boltzmann method for the compressible Euler equations, *Phys. Rev. E.*, 69 (2004), 056702.
- [7] K. Qu, C. Shu and Y. T. Chew, Alternative method to construct equilibrium distribution functions in lattice-Boltzmann method simulation of inviscid compressible flows at high Mach number, *Phys. Rev. E.*, 75 (2007), 036706.
- [8] F. J. Alexander, S. Chen and J. D. Sterling, Lattice Boltzmann thermohydrodynamics, *Phys. Rev. E.*, 47 (1993), R2249–R2252.
- [9] Y. Chen, H. Ohashi and M. Akiyama, Thermal lattice Bhatnagar-Gross-Krook model without nonlinear deviations in macrodynamic equations, *Phys. Rev. E.*, 50 (1994), 2776–2783.
- [10] C. Sun, Lattice Boltzmann models for high speed flows, *Phys. Rev. E.*, 58 (1998), 7283–7287.
- [11] C. Sun, Adaptive lattice Boltzmann model for compressible flows: viscous and conductive properties, *Phys. Rev. E.*, 61 (2000), 2645–2653.
- [12] C. Sun and A. T. Hsu, Three-dimensional lattice Boltzmann model for compressible flows, *Phys. Rev. E.*, 68 (2003), 016303.
- [13] C. Sun and A. Hsu, Multi-level lattice Boltzmann model on square lattice for compressible flows, *Comput. Fluids.*, 33 (2004), 1363–1385.
- [14] M. Watari and M. Tsutahara, Two-dimensional thermal model of the finite-difference lattice Boltzmann method with high spatial isotropy, *Phys. Rev. E.*, 67 (2003), 036306.

- [15] M. Watari, Finite difference lattice Boltzmann method with arbitrary specific heat ratio applicable to supersonic flow simulations, *Phys. A.*, 382 (2007), 502–522.
- [16] T. Kataoka and M. Tsutahara, Lattice Boltzmann model for the compressible Navier-Stokes equations with flexible specific-heat ratio, *Phys. Rev. E.*, 69 (2004), 035701.
- [17] G. Yan, J. Zhang, Y. Liu and Y. Dong, A multi-energy-level lattice Boltzmann model for the compressible Navier-Stokes equations, *Int. J. Numer. Meth. Fluids*, 55 (2007), 41–56.
- [18] X. Pan, A. Xu, G. Zhang and S. Jiang, Lattice Boltzmann approach to high-speed compressible flows, *Int. J. Mod. Phys. C.*, 18 (2007), 1747–1764.
- [19] Y. Gan, A. Xu, G. Zhang, X. Yu and Y. Li, Two-dimensional lattice Boltzmann model for compressible flows with high Mach number, *Phys. A.*, 387 (2008), 1721–1732.
- [20] Q. Li, Y. He, Y. Wang and W. Tao, Coupled double-distribution-function lattice Boltzmann method for the compressible Navier-Stokes equations, *Phys. Rev. E.*, 76 (2007), 056705.
- [21] Y. Wang, Y. He and Q. Li, Lattice Boltzmann model for viscous compressible flows with high Mach number, *ASCHT2007-139*.
- [22] Q. Li, Y. He and Y. Gao, Implementation of finite-difference lattice Boltzmann method on general body-fitted curvilinear coordinates, *Int. J. Mod. Phys. C.*, 19 (2008), 1581–1595.
- [23] C. M. Teixeira, Incorporating turbulence models into the lattice-Boltzmann method, *Int. J. Mod. Phys. C.*, 9 (1998), 1159–1175.
- [24] O. Filippova, S. Succi, F. Mazzocco, C. Arrighetti, G. Bella and D. Hanel, Multiscale lattice Boltzmann schemes with turbulence modeling, *J. Comput. Phys.*, 170 (2001), 812–829.
- [25] T. Imamura, K. Suzuki, T. Nakamura and M. Yoshida, Flow simulation around an airfoil using lattice Boltzmann method on generalized coordinates, *AIAA-2004-244*.
- [26] R. A. Shock, S. Mallick, H. Chen, V. Yakhot and R. Zhang, Recent results on two-dimensional airfoils using a lattice Boltzmann-based algorithm, *J. Aircraft.*, 39 (2002), 434–439.
- [27] Y. Zhou, R. Zhang, I. Staroselsky and H. Chen, Numerical simulation of laminar and turbulent buoyancy-driven flows using a lattice Boltzmann based algorithm, *Int. J. Heat. Mass. Tran.*, 47 (2004), 4869–4879.
- [28] Y. Li, R. Shock, R. Zhang and H. Chen, Simulation of turbulent flow in a cyclonic separator with lattice Boltzmann method, *AIAA-2006-3903*.
- [29] R. Satti, Y. Li, R. Shock and S. Hoelting, Simulation of flow over a 3-element airfoil using a lattice-Boltzmann method, *AIAA-2008-549*.
- [30] A. Keating, J. Beedy and R. Shock, Lattice Boltzmann simulations of the DLR-F4, DLR-F6 and variants, *AIAA-2008-749*.
- [31] P. R. Spalart and S. R. Allmaras, A one-equation turbulence model for aerodynamic flows, *AIAA-92-0439*.
- [32] C. Gacherieu and C. Weber, Assessment of algebraic and one-equation turbulence models for transonic turbulent flow around a full aircraft configuration, *AIAA-98-2737*.
- [33] S. Deck, P. Duveau, P. d’Espiney and P. Guillen, Development and application of Spalart Allmaras one equation turbulence model to three dimensional supersonic complex configurations, *Aerosp. Sci. Technol.*, 6 (2002), 171–183.
- [34] Y. H. Qian, D. d’Humières and P. Lallemand, Lattice BGK models for Navier-Stokes equation, *Europhys. Lett.*, 17 (1992), 479–484.
- [35] J. D. Anderson Jr., *Computational Fluid Dynamics: The Basics with Applications*, Beijing: Tsinghua University Press, 2002.
- [36] Z. Guo, C. Zheng, B. Shi and T. S. Zhao, Thermal lattice Boltzmann equation for low Mach number flows: decoupling model, *Phys. Rev. E.*, 75 (2007), 036704.
- [37] S. Pieraccini and G. Puppo, Implicit-explicit schemes for BGK kinetic equations, *J. Sci. Com-*

- put., 32 (2007), 1–28.
- [38] Z. Zhu, Z. Wu, J. Lin, C. Yan and Z. Chen, *Applied Computational Fluid Dynamics*, Beijing: Beijing University of Aeronautics and Astronautics Press, 1998 (in Chinese).
 - [39] Z. Guo, C. Zheng and B. Shi, Non-equilibrium extrapolation method for velocity and pressure boundary conditions in the lattice Boltzmann method, *Chinese Phys.*, 11 (2002), 366–374.
 - [40] D. D. Marshall and S. M. Ruffin, A new inviscid wall boundary condition treatment for embedded boundary Cartesian grid schemes, AIAA-04-0583.
 - [41] C. Zhong, K. Li, J. Sun, C. Zhuo and J. Xie, Simulation of compressible flow around an airfoil based on lattice Boltzmann method, *Transactions of Nanjing University of Aeronautics and Astronautics*, 26 (2009), 206–211.
 - [42] J. J. Thibert, M. Grandjacques and L. H. Ohman, Experimental database for computer program assessment, AGARD-AR-138, A1 (1979), A1-1–A1-36.
 - [43] J. B. McDevitt and A. F. Okuno, Static and dynamic pressure measurements on a NACA0012 airfoil in the Ames high Reynolds number facility, NASA-TP-2485, 1985.